Applied Catalysis A, General 580 (2019) 46–52

Contents lists available at ScienceDirect

Applied Catalysis A, General

journal homepage: www.elsevier.com/locate/apcata

The roles of nitrogen species on graphene aerogel supported Cu-Zn as efficient catalysts for CO_2 hydrogenation to methanol

Varisara Deerattrakul[a], Nevzat Yigit[b], Günther Rupprechter[b], Paisan Kongkachuichay[a,c,*]

[a] Department of Chemical Engineering, Faculty of Engineering, Kasetsart University, Bangkok 10900, Thailand
[b] Institute of Materials Chemistry, Technische Universität Wien, Getreidemarkt 9/1060, Vienna, Austria
[c] Research Network of NANOTEC–KU on NanoCatalysts and NanoMaterials Sustainable Energy and Environment, Kasetsart University, Bangkok 10900, Thailand

ARTICLE INFO

Keywords:
CO_2hydrogenation
Methanol
Cu-Zn
Graphene
Nitrogen
Aerogel

ABSTRACT

The nitrogen heteroatom has been recently doped into carbon materials such as carbon nanotubes and graphene for enhance the catalytic activity of CO_2 hydrogenation to methanol. However, the role in each of the nitrogen species are not yet fully understood. In this work, the nitrogen has been doped to the graphene aerogel by using different nitrogen sources (i.e., ammonia, hydrazine hydrate, and urea) *via* a hydrothermal reduction method, and the role of each nitrogen species has been investigated. It is found that 15%CuZn loaded on nitrogen doped graphene aerogel catalyst using urea as a precursor provided the highest space-time yield of methanol (405.49 mg g_{cat}^{-1} h^{-1}). Remarkably, the increase of pyridinic nitrogen can greatly promote the catalytic performance and enhance the methanol production. This work is the first systematic study on the influent of nitrogen species doping on graphene aerogel support and also proves that pyridinic-N plays an important role to enhance the catalytic performance.

1. Introduction

Carbon dioxide (CO_2) has been considered as one of the major greenhouse gases, and the increasing CO_2 emission into the atmosphere leads to global climate change. Therefore, the control of CO_2 emission has received much attention worldwide. CO_2 utilization is an effective way to reduce the amount of CO_2 accumulation and convert to value-added products and fuels [1]. CO_2 hydrogenation to methanol is one of the solutions that can contribute to CO_2 emissions mitigation and fossil fuel substitution. Due to the fact that methanol can be used as feedstock for chemicals such as acetic acid, formaldehyde, and methyl tertiary-butyl ether (MTBE), and also alternative fuels such as aromatics, high-octane gasoline, and olefins [2–5]. However, direct methanol synthesis from CO_2 hydrogenation reaction is an exothermic reaction involving kinetic and thermal dynamic limitation [6].

Cu/ZnO based catalysts have been reported as efficient catalysts for CO_2 hydrogenation to methanol process because Cu is often regarded as active sites, and ZnO can increase the Cu dispersion, preventing copper deactivation by sintering and also provide active sites for hydrogen spillover [7–9]. Moreover, it is found that the interactions of Cu and ZnO can improve the direct CO_2 hydrogenation to methanol [10]. However, the activity of catalyst depends on the dispersion of metal nanoparticles and the interaction of support relating to transfer electron from support, which can improve not only the metal dispersion but also increase surface area leading to enhance the catalytic performance [11–13]. Hence, supports play a crucial role to develop the Cu/ZnO based catalysts. Carbon materials—activated carbon [14], carbon nanotubes [15], graphene [16], and so on—have been recognized as excellent catalytic supporters due to their high specific surface area, high thermal stability, and tailored pore structure leading to the flexible design of porous carbon [17]. Großmann et al. [18] applied the multi-walled carbon nanotubes (CNTs) for use as a support for Cu/ZnO catalyst and found that CNTs can expose Cu surface area, which can enhance the methanol productivity (41.4 mg g_{cat}^{-1} h^{-1}). Liakakou et al. [19] reported that the activated carbon support can enhance the selectivity to higher alcohols comparing to the unsupported material, which may be ascribed to better dispersion of active phase. Liang et al. [20] decorated CNT with Pd, which can promote the Pd-ZnO catalyst leading to reach highly the catalyst activity for CO_2 hydrogenation to methanol with the corresponding space-time yield (STY) of methanol being 37.1 mg g_{cat}^{-1} h^{-1}. Furthermore, it is found that carbon nanofiber (CNF) supported Cu/ZrO_2 catalyst exhibited the methanol productivity of 25 mg g_{cat}^{-1} h^{-1} [21]. Recently, we reported the Cu-ZnO supported graphene aerogel in CO_2 hydrogenation to methanol and also found that this catalyst yielded the highest STY of methanol to 94.5 mg g_{cat}^{-1} h^{-1} [22].

* Corresponding author at: Department of Chemical Engineering, Faculty of Engineering, Kasetsart University, Bangkok 10900, Thailand.
E-mail address: paisan.k@ku.ac.th (P. Kongkachuichay).

https://doi.org/10.1016/j.apcata.2019.04.030
Received 24 January 2019; Received in revised form 16 April 2019; Accepted 27 April 2019
Available online 30 April 2019
0926-860X/

It is obvious that graphene is a good candidate for catalyst support for CO_2 hydrogenation to methanol due to its great properties such as large theoretical surface area (2630 $m^2 g^{-1}$) [23,24], good electron mobility (15,000 $cm^2 V^{-1}$) [25], high mechanical strength (130 GPa) [26], high thermal stability (600 °C in air) [27], and easy to functionalize with heteroatoms (i.e., boron, nitrogen, sulfur, and phosphorus) [28–30]. Unfortunately, graphene can restack into a graphite form leading to poor specific surface area (~117 to 458 $m^2 g^{-1}$) [16,22,31].

In order to enhance methanol productivity, the nitrogen groups have been recently doped into the carbon-based supports. It has been reported that the nitrogen might play a significant role for a stronger interaction of CO_2 molecules and facilitate the metal dispersion [32,33]. Sun *et al.* [34] prepared the nitrogen-doped CNTs supported Cu-ZrO_2 and found that the doped nitrogen species can enhance the methanol yield (up to 102.21 mg $g_{cat}^{-1} h^{-1}$). More convincing work was reported by Wu *et al.* [35]. They studied the role of nitrogen species in nitrogen-doped graphene quantum dots as a metal-free catalyst and reported that nitrogen dopants promote the CO_2 hydrogenation activity leading to lower temperature of CO_2 reduction and improve CO_2 conversion as well as CH_4 selectivity. Chew *et al.* [36] reported that the presence of nitrogen functionality on CNTs support enhances the reduction of iron oxide, which is a key for promoting the catalytic performance in CO_2 hydrogenation. Moreover, Kumar *et al.* [37] found that the doping of nitrogen in graphene can transfer the electron to convert CO_2 to methanol under the visible light irradiation and also provide the surface to bond with metal complex and CO_2.

Previously, we also introduced the nitrogen into Cu-ZnO/graphene catalyst. Obviously, we have found that the nitrogen plays an important role to enhance the methanol production up to 591 mg $g_{cat}^{-1} h^{-1}$ [16,38], compared to that of without nitrogen (94.5 mg $g_{cat}^{-1} h^{-1}$). However, the roles of nitrogen: pyridinic-N, pyrrolic-N, and graphitic-N in graphene structure for CO_2 hydrogenation to methanol has not yet been fully understood. Herein, we provide the first demonstration of the role of pyridinic-N in Cu-ZnO/N-doped graphene aerogel catalyst for CO_2 hydrogenation to methanol. This work improves understanding of the characteristic of pyridinic-N, which is an important key for the improvement of Cu-Zn catalysts and related catalyst families.

2. Experimental

2.1. Chemicals and materials

Graphite powder (20–40 μm, Sigma Aldrich), sulfuric acid (98% H_2SO_4, QRec), potassium permanganate (99% $KMnO_4$, Ajax Finechem), sodium nitrate (99.5% $NaNO_3$, QRec), hydrogen peroxide (30% H_2O_2, Merck), ammonium hydroxide (28% NH_4OH, QRec), hydrazine hydrate (80% N_2H_4, Merck), urea (NH_2CONH_2, Ajax Finechem), copper nitrate trihydrate (99.5% $Cu(NO_3)_2{\cdot}3H_2O$, QRec), zinc nitrate hexahydrate (98% $Zn(NO_3)_2{\cdot}6H_2O$, Lobachemie), and water purified by using the Milli-Q system (< 18 MΩ cm, Millipore) were used in this work.

2.2. Synthesis of graphite oxide

Graphite oxide (GO) was synthesized by the modified Hummer's method [39]. Briefly, graphite powder (5.0 g) and $NaNO_3$ (7.5 g) were dissolved into H_2SO_4 (500 ml) under stirring (200 rpm). Then, $KMnO_4$ (40.0 g) was slowly added to the suspension under stirring in an ice bath and kept stirring for 24 h. Next, the distilled water (500 ml) and H_2O_2 (150 ml) were slowly added into the suspension under stirring for 24 h. After that, GO was collected by centrifugal, washed with distilled water several times, and then dried at 50 °C for 24 h.

2.3. Synthesis of nitrogen-doped reduced graphene oxide aerogel

The nitrogen-doped reduced graphene oxide aerogel ($NrGO_{ae}$) was synthesized via a facile one-pot hydrothermal procedure with different reducing agents: ammonium hydroxide, hydrazine hydrate and urea to produce a three-dimensional (3D) interconnected framework. $NrGO_{ae}$ was synthesized via the same synthesis route of reduced graphene oxide aerogel (rGO_{ae}), which has been described in our previous work [22]. Briefly, 2 mg ml^{-1} suspension of GO in deionized water was sonicated for 2 h to obtain the graphene oxide. Then, the mixture was placed into a Teflon-line autoclave and maintained at 140 °C for 24 h to form reduced graphene oxide (rGO) hydrogel. After that, the autoclave was naturally cooled down to room temperature. Finally, the as-synthesized rGO hydrogel was frozen at 0 °C for 24 h and freeze-dried for 72 h to obtain rGO_{ae}. In order to prepare $NrGO_{ae}$, 0.5 M of ammonium hydroxide, hydrazine hydrate, and urea was added into the GO aqueous suspension before transfer to a Teflon-line autoclave. Afterwards, the as-prepared hydrogel was washed with Milli-Q water in order to get rid of the residual reducing agent. Then, the as-synthesized NrGO hydrogel was frozen and freeze-dried. The final product aerogel was labeled as $NrGO_{ae}$-A, $NrGO_{ae}$-H and $NrGO_{ae}$-U (A, H, and U indicate ammonium hydroxide, hydrazine hydrate, and urea reduction, respectively).

2.4. Synthesis of Cu-Zn/nitrogen-doped reduced graphene oxide aerogel

The 15 wt% of Cu-Zn/N-rGO were prepared by incipient wetness impregnation with equimolar concentrations of Cu and Zn [22]. Subsequently, the as-synthesized catalysts were dried at 100 °C for 12 h and calcined in air at 350 °C for 2 h with a heating rate of 2 °C min^{-1} to remove impurities and decompose metal salts to be metal oxides (i.e., CuO and ZnO) [16,22,38].

2.5. Characterization of catalysts

The morphology of all samples was characterized by a field-emission scanning electron microscope (FE-SEM: JEOL, JSM-7600 F) with an accelerating voltage of 5 kV and Pt-coated (thickness of 2 nm), and a transmission electron microscope (TEM; JEOL JEM-3100 F) operating at 300 kV. To prepare the samples for TEM analysis, the samples suspended in ethanol were sonicated and then coated on a copper grid. X-ray diffraction (XRD: Philips X'Pert) was used to analyze the structure of the as-prepared samples by using Cu-K_α radiation (λ = 1.54 Å) operating in the range from 5° to 90° at 40 kV and 30 mA. The Brunauer-Emmett-Teller (BET) surface area was examined by the nitrogen adsorption-desorption method at −196 °C using a Quantachrome Autosorb-1C instrument. Before the measurement, samples were degassed at 100 °C for 12 h. The functional groups of the catalysts were investigated by Fourier transform infrared spectroscopy (FTIR: Bruker TENSOR 27) equipped with a DTGs detector in the 400–4000 cm^{-1} region with a resolution of 4 cm^{-1}. The Raman spectra were recorded by Raman spectroscopy (Senterra dispersive Raman microscope: Bruker Optics) with an excitation laser of 532 nm. To investigate the thermal stability and the decomposition of the as-prepared samples, a thermogravimetric analyzer (TGA: Perkin Elmer) was performed under flowing of air (100 ml min^{-1}) at a heating rate of 10 °C min^{-1} in the temperature range from 25 to 600 °C. H_2 temperature programmed desorption (H_2-TPD) was carried out on a quadrupole mass spectrometer (Balzers Prisma 260) to monitor desorption of H_2. All samples (0.05 g) were evacuated at 150 °C for 1 h and then cooled to room temperature. After that, they were saturated in H_2 for 1 h at room temperature. Finally, desorption process was recorded with a heating rate of 5 °C min^{-1} under vacuum. Furthermore, CO_2 temperature programmed desorption (CO_2-TPD) was measured in the same way as that of H_2-TPD. The surface chemical compositions of the as-prepared samples were characterized by X-ray photoelectron spectroscopy (XPS: AXIS Ultra DLD, Kratos Analytical Ltd.). The atomic concentrations of elements were examined by the integration of the peak. The reducibility of the catalyst was characterized by H_2-TPR technique under feed gas of 9.6% H_2 balanced with Ar in the range of 25–800 °C.

2.6. Catalytic performance test

Catalyst testing at 250 °C and 15 bar with a CO_2/H_2 (1/3) mixture at GHSV of 2444 h^{-1} was operated in a tubular stainless steel fixed-bed reactor. 0.15 g of catalyst was loaded to the reactor. Before the reaction, the catalyst was in-situ reduced at 350 °C under atmospheric pressure with flowing H_2 (40 ml min^{-1}) for 1.5 h. Then, the gaseous product was performed using an online GC-14 A gas chromatography equipped in a Unibead-C packed column with thermal conductivity detector (TCD) and a Porapak Q column with flame ionization detector (FID). The STY of methanol (mg g_{cat}^{-1} h^{-1}) was examined as follows:

$$\text{STY of methanol} = \frac{\text{moles methanol}}{\text{amount of catalyst} \times V_{sampling}} \times \dot{V}_{total} \times MW_{methanol} \quad (1)$$

where $\dot{V}_{total}$ and $V_{sampling}$ are the total volumetric flow of CO_2 and H_2 mixtures and the volume of sampling for GC, respectively. $MW_{methanol}$ is the molecular weight of methanol (32 g mol^{-1}).

3. Results and discussion

To investigate the morphologies of Cu-Zn metals on $NrGO_{ae}$ supports prepared with different reducing agents (i.e., ammonium hydroxide, hydrazine hydrate, and urea). The catalysts were examined by FE-SEM (Fig. 1 a–c) and TEM (Fig. 1d–f and Fig. S2). It is clear that the Cu-Zn particles are well dispersed in the internal and external porous frameworks of all $NrGO_{ae}$ supports (including $NrGO_{ae}$-A, $NrGO_{ae}$-H and $NrGO_{ae}$-U), resulting in the creation of polarity by nitrogen atoms [37]. Moreover, it can be found that some large agglomeration of particles are seen in Fig. 1a (15%CuZn/$NrGO_{ae}$-A) following by Fig. 1b (15%CuZn/$NrGO_{ae}$-H). Besides, it is difficult to observe any particles in Fig. 1c (15%CuZn/$NrGO_{ae}$-U). This may be due to very small particle size. Thus, the order of the particle sizes observed in Fig. 1a–c would be 15%CuZn/$NrGO_{ae}$-A > 15%CuZn/$NrGO_{ae}$-H > 15%CuZn/$NrGO_{ae}$-U. Furthermore, TEM images of all catalysts display a good agreement with the FE-SEM images, showing that all $NrGO_{ae}$ exhibit many wrinkles with good dispersion of copper and zinc particles. Furthermore, the average sizes of Cu-Zn nanoparticles supported on $NrGO_{ae}$-A, $NrGO_{ae}$-H and $NrGO_{ae}$-U are approximately 10–11 nm, 8–9 nm, and 7–8 nm, respectively (see inset images in Fig. 1d–f). The addition of Cu-Zn metals does not destroy the 3D porous network of $NrGO_{ae}$, which can be seen in Fig. S1. After loading Cu-Zn metals, all supports display the same structure and also have high wrinkles and crumpled characters on the surface.

To further understand the physico-chemical properties of Cu-Zn catalyst supported on $NrGO_{ae}$-A, $NrGO_{ae}$-H and $NrGO_{ae}$-U, all catalysts were characterized by XRD, N_2 sorption, FTIR, Raman and TGA techniques and the obtained results are shown in Fig. 2. The XRD patterns of all catalysts (Fig. 2a) display the predominant peak at around 2θ = 25° and a weak peak at around 2θ = 43.2°, related to the diffraction from (002) and (100) planes of rGO, respectively indicating the characteristics of rGO structure [40]. It is clear that the loading of Cu-Zn metals does not destroy the rGO structure (see Fig. S2a for the $NrGO_{ae}$ before metal loading). Furthermore, the crystallite sizes of CuO and ZnO were calculated using the Scherrer equation. It is found that the crystallite sizes of CuO are 7.4, 7.3, and 7.1 nm, and the crystallite sizes of ZnO are 7.5, 7.5, and 7.2 nm for 15%CuZn/$NrGO_{ae}$-A, 15%CuZn/$NrGO_{ae}$-H, and 15%CuZn/$NrGO_{ae}$-U, respectively, which are in the same order of magnitude with the particle sizes obtained from the TEM images (Fig. 1 and Fig. S2). All samples after metal loading present the type IV isotherm with the characteristic H3-type hysteresis loop, indicating the mesoporous structure as shown in Fig. 2b [41]. Moreover, the BET surface areas of as-prepared samples were then calculated from the adsorption isotherm as 259, 259, and 110 $m^2 g^{-1}$ for 15%CuZn/$NrGO_{ae}$-A, 15%CuZn/$NrGO_{ae}$-H, and 15%CuZn/$NrGO_{ae}$-U catalysts, respectively. To analyze the functional groups of the as-synthesized Cu-Zn/$NrGO_{ae}$ with different reducing agents, the FTIR spectra were measured and are shown in Fig. 2c. All samples show the absorption bands at approximately 1556 cm^{-1} and 1195 cm^{-1}, which are attributed to C=C/C=N groups and C−N groups, respectively [42]. This confirms that the nitrogen atoms were successfully doped into the graphene aerogel structure. Moreover, the absorption band at around 400–500 cm^{-1} is associated with the Cu−O and Zn−O stretching mode vibration [43]. In Fig. 2d, Raman spectra of the as-prepared catalysts exhibit two dominant peaks, which are D and G bands, and two minor peaks of 2D and S3 bands. Generally, the D peak at ~1355 cm^{-1} represented the lattice of sp^3 hybridization (breathing mode of A_{1g} symmetry) indicating the defected of the graphene sheet and the carbon atom at the edge orientation. The G band at ~1596 cm^{-1} represents the E_{2g} phonon of the graphitic sp^2 carbon atoms [44,45]. Moreover, the broader peaks of 2D (~2709 cm^{-1}) and S3 (~2912 cm^{-1}) bands can be indicated that the as-prepared catalysts consist of few layers graphene with a structural defect, which may result from the nitrogen impurities [46]. In the inset of Fig. 2d, the obvious peak at 113.0 cm^{-1} and a

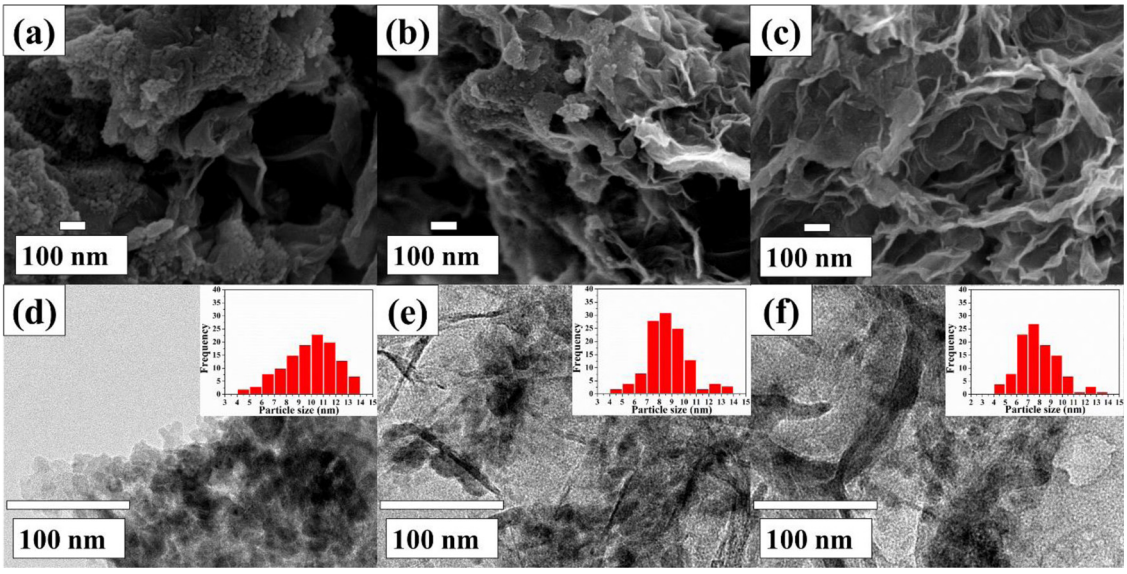

Fig. 1. Surface morphology of the as-prepared catalysts: FE-SEM images of (a) 15%CuZn/$NrGO_{ae}$-A, (b) 15%CuZn/$NrGO_{ae}$-H, (c) 15%CuZn/$NrGO_{ae}$-U; and TEM images of (d) 15%CuZn/$NrGO_{ae}$-A, (e) 15%CuZn/$NrGO_{ae}$-H, (f) 15%CuZn/$NrGO_{ae}$-U.

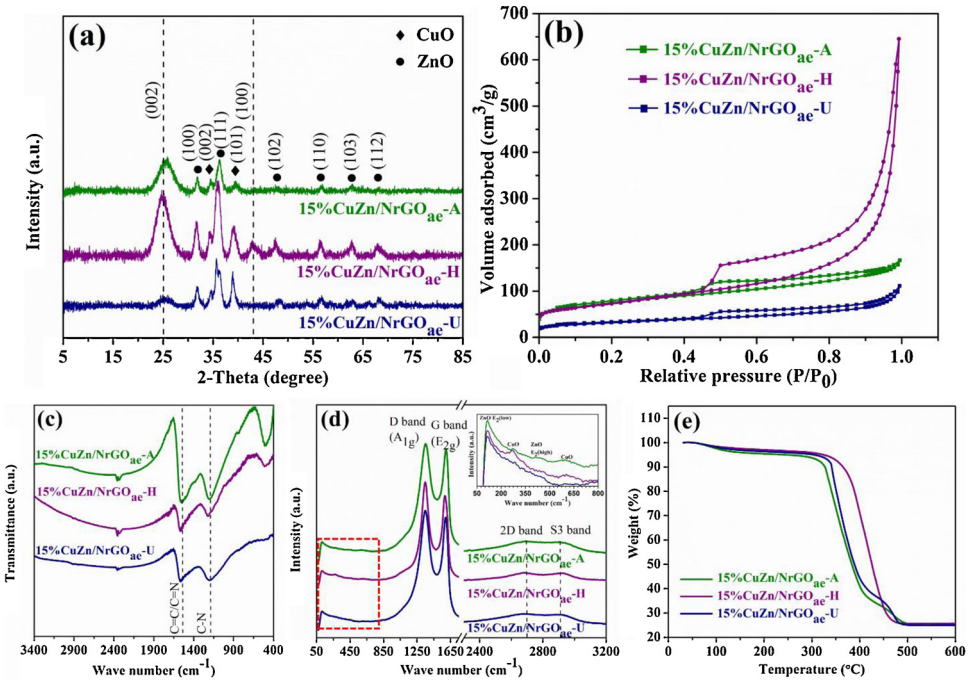

Fig. 2. Physico-chemical properties of the as-prepared catalysts (a) XRD patterns, (b) N_2 sorption isotherms, (c) FTIR spectra, (d) Raman spectra, and (e) TGA profiles.

minor peak at 429.0 cm^{-1} considering in ZnO mode are attributed to E_2 low vibration mode (refer to Zn sub-lattice) and E_2 high vibration mode (refer to oxygen atoms), respectively [47]. The peaks at 275.5 cm^{-1} and 611.5 cm^{-1} are associated with the crystalline structure of CuO [48,49]. The thermal behaviour of the as-prepared catalysts was investigated by thermogravimetric analysis (TGA) in the air as shown in Fig. 2e. It can be clearly seen that the weight loss of as-prepared catalysts is about 5% in the range from room temperature to below 150 °C corresponding to the removal of adsorbed water. The sudden weight loss occurs in the range of 350 °C–500 °C. After 500 °C, the NrGO$_{ae}$ supports completely decomposed. Moreover, the as-prepared catalysts provide the same ash content about 25 wt%, which confirms the equal amount of Cu-Zn metal loading (i.e., 15 wt%) of all as-prepared catalysts. Note, the TGA profiles of NrGO$_{ae}$ supports can be found in Fig. S3e.

H_2-TPD profiles of all catalysts with the different reducing agents are shown in Fig. 3a. There are two desorption peaks observed for all catalysts. The minor H_2 desorption peaks at lower temperature in the range of 100–175 °C are ascribed to the hydrogen spillover with H_2 dissociating on Cu sites [50,51], whereas the major H_2 desorption peaks at higher temperature are attributed to the desorption of adsorbed hydrogen from ZnO surface, and from Cu-ZnO interface [52]. Moreover, the quantity of desorbed H_2 at low temperature is about 7.503, 7.503 and 7.504 μmol for 15%CuZn/NrGO$_{ae}$-A, 15%CuZn/NrGO$_{ae}$-H and 15%CuZn/NrGO$_{ae}$-U, respectively (see the calibration curve in Fig. S6). Besides, the quantity of desorbed H_2 at high temperature is around 7.541, 7.545 and 7.558 μmol for 15%CuZn/NrGO$_{ae}$-A, 15%CuZn/NrGO$_{ae}$-H and 15%CuZn/NrGO$_{ae}$-U, respectively. The 15%CuZn/NrGO$_{ae}$-U catalyst provides the highest quantity of desorbed H_2, which may result from the presence of pyridinic-N. The basicity of all catalysts was examined by CO_2-TPD, and the obtained results are shown in Fig. 3b (see Fig. S7 for CO_2-TPD profile of supports). All catalysts show broader peaks in the range of 250–500 °C attributing to strongly basic sites, which is associated with the active site for CO_2 activation [53,54].

The surface chemistry of the catalysts and NrGO$_{ae}$ supports was studied by using an XPS, and the obtained spectra of all samples are presented in Fig. 4, Fig. S4, and Fig. S5. All samples show a major C1s peak at 284.5 eV, a minor O1s peak at 531.5 eV, and nitrogen (N1s) at 399.5 eV [55]. The copper peaks (Cu2p, 934.5–963.2 eV) [56] and zinc peaks (Zn2p (1022.3 and 1045.3 eV), Zn3s (140.5 eV), and Zn3p (91.5 eV)) were detected when loading with Cu-Zn metals [56,57]. There are no any impurities found in all samples. To understand the

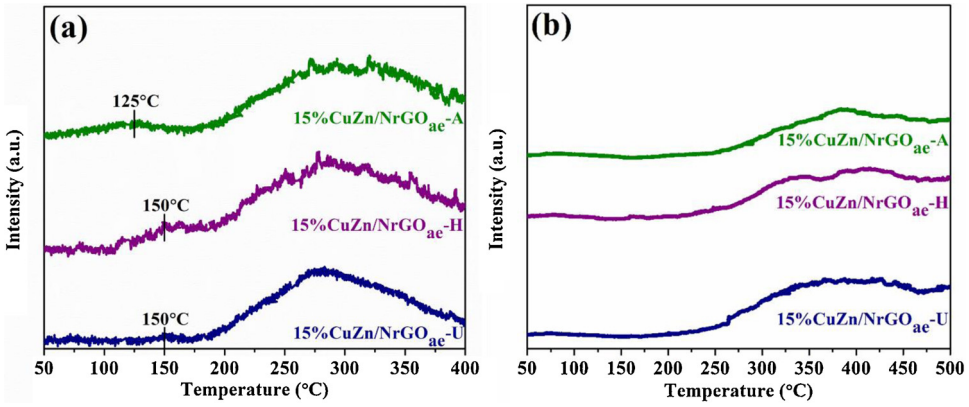

Fig. 3. (a) H_2-TPD profiles and (b) CO_2-TPD profiles of the as-prepared catalysts.

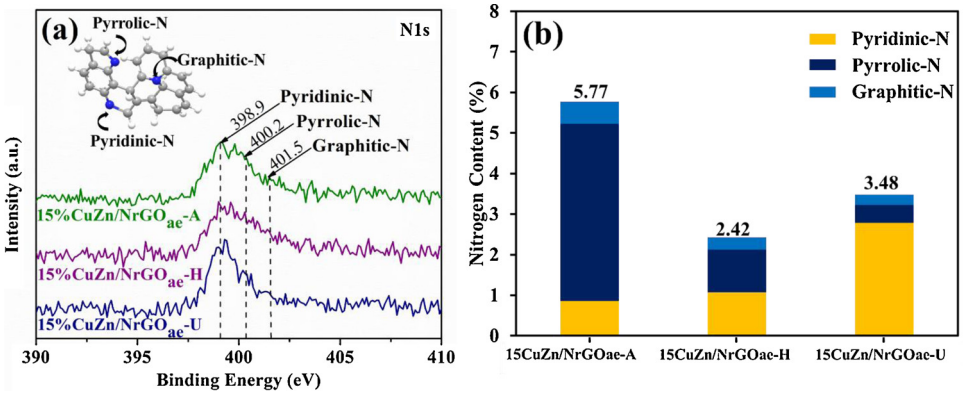

Fig. 4. (a) High resolution N1s XPS spectra and (b) specific nitrogen contents of the as-prepared catalysts.

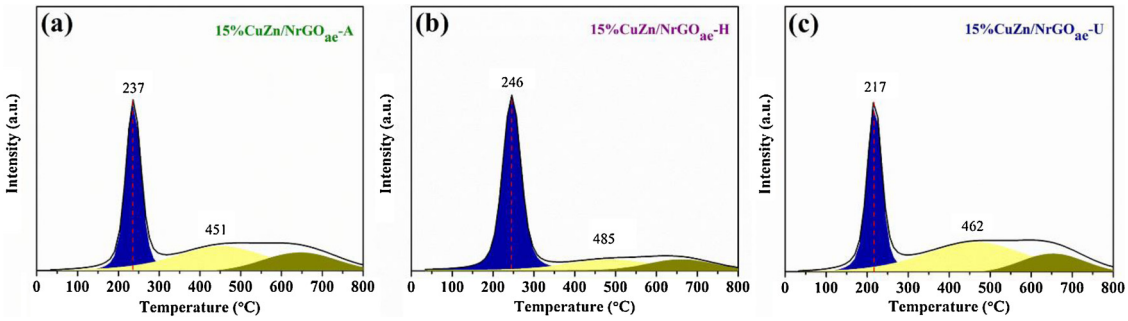

Fig. 5. H_2-TPR profiles of (a) 15%CuZn/NrGO$_{ae}$-A, (b) 15%CuZn/NrGO$_{ae}$-H, and (c) 15%CuZn/NrGO$_{ae}$-U.

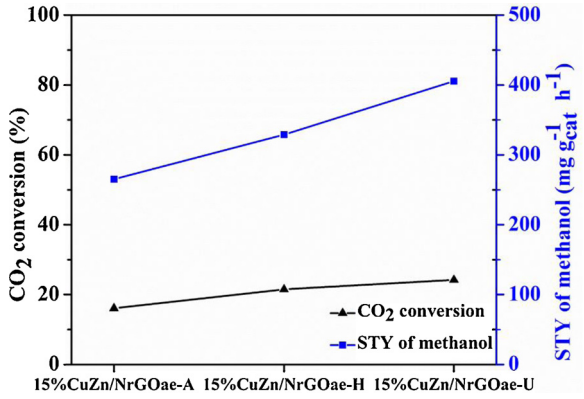

Fig. 6. CO_2 conversion and space-time yield of methanol at 250 °C and 15 bar of CO_2.

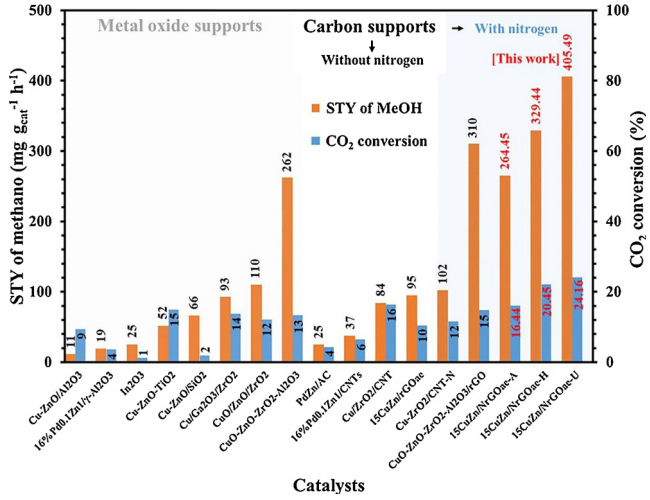

Fig. 7. Comparison of the space-time yield and CO_2 conversion with previous works [20,31,34,68–74].

chemical bonding of the specific nitrogen species, the N1s peak of the supported Cu-Zn on NrGO$_{ae}$ catalysts was deconvoluted by XPS PEAK 4.1 software as shown in Fig. S8. According to Fig. 4a, it can be classified the spectra into three peeks: (1) pyridinic-N at ~398.9 eV (the nitrogen atom connecting to two carbon atoms in a benzene ring), (2) pyrrolic-N at ~400.2 eV (the nitrogen atom connecting to two C atoms in a pentagon ring), and (3) graphitic-N at ~401.5 eV (the nitrogen atom substituting the carbon atoms in a benzene ring) [58,59]. In Fig. 4b, it is found that by changing the nitrogen source gives the different amount of nitrogen contents, which are 5.77, 2.42, and 3.48 at% for 15%CuZn/NrGO$_{ae}$-A, 15%CuZn/NrGO$_{ae}$-H and 15%CuZn/NrGO$_{ae}$-U catalysts, respectively. The presence of nitrogen in graphene aerogel gave a smaller size of metal particles comparing to that of without nitrogen doped [22]. This is due to the promoting electronic structure of NrGO$_{ae}$ leading to improve the metal dispersion [60]. Moreover, it is obvious that the 15%CuZn/NrGO$_{ae}$-U catalyst displays the highest pyridinic-N content up to 2.78 at%. The pyridinic-N is then decreased to 1.06 and 0.86 at% for 15%CuZn/NrGO$_{ae}$-H and 15%CuZn/NrGO$_{ae}$-A catalysts, respectively. Furthermore, nitrogen, especially pyridinic-N, on supports can donate an electron, which impacts on the binding between catalyst and support leading to prevent the metal agglomeration and reduced the coarsening action [61,62], and also can facilitate the H_2 dissociation and promote CO_2 adsorption leading to improvement of catalytic performance [63].

Fig. 5 shows the reducibility of CuO and ZnO supported on NrGO$_{ae}$ measured by H_2-TPR technique. The predominant peak at low temperature represents the reduction of CuO species, which are highly dispersed CuO, bulked CuO, [64]. Then, the high-temperature reduction peaks are attributed to the reduction of partial ZnO and NrGO$_{ae}$ [65,66]. Notably, increasing nitrogen content leads to the lower

reduction temperature of CuO, due to the fact that doping nitrogen can donate an electron to CuO and promote the CuO reduction [67]. However, it is clear that different degree of aggregation is observed on SEM and TEM images. Thus, the effect of particle size maybe involves the different reducibility. Furthermore, the relative surface-dispersed CuO concentration (C) was approximately calculated from the peak areas (A) of CuO species by the following equation:

$$C = \frac{A_{\text{surface-dispersed CuO}}}{(A_{\text{surface-dispersed CuO}} + A_{\text{bulk CuO}})} \quad (2)$$

A reduction of CuO species at low temperature can be deconvoluted into two peaks as shown in Fig. S9. The result shows that the relative surface-dispersed CuO concentrations are 38.2%, 39.9% and 43.7% for 15%CuZn/$NrGO_{ae}$-A, 15%CuZn/$NrGO_{ae}$-H and 15%CuZn/$NrGO_{ae}$-U, respectively. Moreover, the relative surface-dispersed CuO concentration of 15%CuZn/$NrGO_{ae}$-U is the highest leading to high catalytic performance.

In order to study the effect of nitrogen species by changing the nitrogen reducing agents of CuZn/$NrGO_{ae}$ catalysts, the catalysts were tested in CO_2 hydrogenation to methanol (See Fig. 6). It is noticeable that the STY of methanol is related to the content of pyridinic-N due to the fact that STY of methanol are found the highest values of 405.49 mg $g_{cat}^{-1} h^{-1}$ with the highest pyridinic-N content of 2.78 at% for 15%CuZn/NrGOae-U catalyst, and then decrease to 329.44 and 264.45 mg $g_{cat}^{-1} h^{-1}$ with the pyridinic-N content reduces to 1.06 and 0.86 at% for 15%CuZn/NrGOae-H and 15%CuZn/NrGOae-A catalysts, respectively. Therefore, it can be concluded that the pyridinic-N can promote methanol productivity due to the fact that it can facilitate H_2 dissociation and contribute to the strong CO_2 adsorption. Furthermore, it is also found that pyridinic-N could help the dispersion of CuO leading to easier reduce at a lower temperature resulting in an enhancement of methanol production. In addition, CO_2 conversion was found to be 16.44, 20.45, and 24.16% over 15%CuZn/$NrGO_{ae}$-A, 15%CuZn/$NrGO_{ae}$-H and 15%CuZn/$NrGO_{ae}$-U catalysts, respectively.

The obtained STY of methanol by this work is compared to those of previous works as shown in Fig. 7. It is obvious that the nitrogen-doped carbon supports can provide up to 4 times higher STY_{MeOH} of methanol than that of undoped carbon materials. The comparative results show that the STY_{MeOH} of this work is higher than that of other works, which is the result from promoting the nitrogen species (especially in the form of pyridinic-N) by promoting the reduction of CuO, adsorption of CO_2, and dissociation of H_2.

4. Conclusions

The nitrogen content was introduced into the Cu-Zn/graphene aerogel catalyst *via* a simple hydrothermal reduction method by using the different reducing agents. It is found that the presence of nitrogen species is related to the catalytic performance in CO_2 hydrogenation to methanol. The pyridinic-N plays a significant role to enhance the catalytic performance by improving the metals dispersion, increasing H_2 dissociation, and boosting CO_2 activation to methanol formation. Obviously, the CuZn/$NrGO_{ae}$-U catalyst yielded the highest STY of methanol (405.49 mg $g_{cat}^{-1} h^{-1}$) due to the presence of the highest pyridinic-N content. This value is higher than those of CuZn supported on $NrGO_{ae}$-A and $NrGO_{ae}$-H. This work provides a clear evidence of the nitrogen roles in CO_2 hydrogenation to methanol.

Acknowledgements

This research was financially supported by the Thailand Research Fund (TRF) through the Royal Golden Jubilee Ph.D. Program (Grant No. PHD/0084/2559 for V. Deerattrakul) and partially supported by the National Nanotechnology Center (NANOTEC), NSTDA, Ministry of Science and Technology, Thailand through its program of Research Network NANOTEC (RNN) and the Kasetsart University Research and Development Institute (KURDI) (for P. Kongkachuichay). G. Rupprechter acknowledges the Austrian Science Fund (FWF) [DK +Solids4Fun W1243].

Appendix A. Supplementary data

Supplementary material related to this article can be found, in the online version, at doi:https://doi.org/10.1016/j.apcata.2019.04.030.

References

[1] A. Bansode, A. Urakawa, J. Catal. 309 (2014) 66–70.
[2] G.A. Olah, A. Goeppert, G.K.S. Prakash, J. Org. Chem. 74 (2) (2009) 487–498.
[3] G.A. Olah, Angew. Chem. Int. Ed. 44 (18) (2005) 2636–2639.
[4] X. Guo, D. Mao, S. Wang, G. Wu, G. Lu, Catal. Commun. 10 (2009) 1661–1664.
[5] W. Wang, S. Wang, X. Ma, J. Gong, Chem. Soc. Rev. 40 (2011) 3703–3727.
[6] S.G. Jadhav, P.D. Vaidya, B.M. Bhanage, J.B. Joshi, Chem. Eng. Res. Des. 92 (2014) 2557–2567.
[7] A. Karelovic, P. Ruiz, Catal. Sci. Technol. 5 (2015) 869–881.
[8] J. Bao, Z. Liu, Y. Zhang, N. Tsubaki, Catal. Commun. 9 (2008) 913–918.
[9] C. Baltes, S. Vukojević, F. Schüth, J. Catal. 258 (2008) 334–344.
[10] F. Arena, G. Mezzatesta, G. Zafarana, G. Trunfio, F. Frusteri, L. Spadaro, J. Catal. 300 (2013) 141–151.
[11] C.J.H. Jacobsen, S. Dahl, P. Hansen, E. Törnqvist, L. Jensen, H. Topsøe, D.V. Prip, P.B. Møenshaug, I. Chorkendorff, J. Mol. Catal. A: Chem. 163 (2000) 19–26.
[12] J. Xiao, D. Mao, X. Guo, J. Yu, Appl. Surf. Sci. 338 (2015) 146–153.
[13] L. Angelo, K. Kobl, L.M.M. Tejada, Y. Zimmermann, K. Parkhomenko, A.-C. Roger, C. R. Chim. 18 (2015) 250–260.
[14] J. Cai, Y. Huang, Y. Guo, Appl. Catal. B 150–151 (2014) 230–237.
[15] B. Wu, Y. Kuang, X. Zhang, J. Chen, Nano Today 6 (2011) 75–90.
[16] V. Deerattrakul, P. Dittanet, M. Sawangphruk, P. Kongkachuichay, J. CO_2 Util. 16 (2016) 104–113.
[17] N. Mager, N. Meyer, A.F. Léonard, N. Job, M. Devillers, S. Hermans, Appl. Catal. B 148–149 (2014) 424–435.
[18] D. Großmann, A. Dreier, C. Lehmann, W. Grünert, Appl. Catal. A 504 (2015) 351–360.
[19] E.T. Liakakou, E. Heracleous, K.S. Triantafyllidis, A.A. Lemonidou, Appl. Catal. B 165 (2015) 296–305.
[20] X.-L. Liang, X. Dong, G.-D. Lin, H.-B. Zhang, Appl. Catal. B 88 (2009) 315–322.
[21] I.U. Din, M.S. Shaharun, A. Naeem, S. Tasleem, M.R. Johan, J. CO_2 Util. 21 (2017) 145–155.
[22] V. Deerattrakul, P. Puengampholsrisook, W. Limphirat, P. Kongkachuichay, Catal. Today 314 (2018) 154–163.
[23] A.R. Kumarasinghe, L. Samaranayake, F. Bondino, E. Magnano, N. Kottegoda, E. Carlino, U.N. Ratnayake, A.A.P. de Alwis, V. Karunaratne, G.A.J. Amaratunga, J. Phys. Chem. 117 (2013) 9507–9519.
[24] P. Iamprasertkun, W. Hirunpinyopas, A.M. Tripathi, M.A. Bissett, R.A.W. Dryfe, Electrochim. Acta 307 (2019) 176–187.
[25] A.K. Geim, K.S. Novoselov, Nat. Mater. 6 (2007) 183.
[26] C. Lee, X. Wei, J.W. Kysar, J. Hone, Science 321 (2008) 385.
[27] Z.-S. Wu, W. Ren, L. Gao, J. Zhao, Z. Chen, B. Liu, D. Tang, B. Yu, C. Jiang, H.-M. Cheng, ACS Nano 3 (2009) 411–417.
[28] Y. Zhao, L. Yang, S. Chen, X. Wang, Y. Ma, Q. Wu, Y. Jiang, W. Qian, Z. Hu, J. Am. Chem. Soc. 135 (2013) 1201–1204.
[29] T. Alizadeh, F. Ahmadian, Anal. Chim. Acta 897 (2015) 87–95.
[30] C.H. Choi, S.H. Park, S.I. Woo, ACS Nano 6 (2012) 7084–7091.
[31] Y.J. Fan, S.F. Wu, J. CO_2 Util. 16 (2016) 150–156.
[32] G.-P. Hao, W.-C. Li, D. Qian, A.-H. Lu, Adv. Mater. 22 (2010) 853–857.
[33] J. Masa, W. Xia, M. Muhler, W. Schuhmann, Angew. Chem. Int. Ed. 54 (2015) 10102–10120.
[34] Y. Sun, L. Chen, Y. Bao, G. Wang, Y. Zhang, M. Fu, J. Wu, D. Ye, Catal. Today 307 (2018) 212–223.
[35] J. Wu, C. Wen, X. Zou, J. Jimenez, J. Sun, Y. Xia, M.-T. Fonseca Rodrigues, S. Vinod, J. Zhong, N. Chopra, I.N. Odeh, G. Ding, J. Lauterbach, P.M. Ajayan, ACS Catal. 7 (2017) 4497–4503.
[36] L.M. Chew, P. Kangvansura, H. Ruland, H.J. Schulte, C. Somsen, W. Xia, G. Eggeler, A. Worayingyong, M. Muhler, Appl. Catal. A 482 (2014) 163–170.
[37] P. Kumar, H.P. Mungse, O.P. Khatri, S.L. Jain, RSC Adv. 5 (2015) 54929–54935.
[38] V. Deerattrakul, W. Limphirat, P. Kongkachuichay, J. Taiwan Inst. Chem. Eng. 80 (2017) 495–502.
[39] W.S. Hummer, R.E. Offema, (1958) 1339.
[40] Y. Xu, K. Sheng, C. Li, G. Shi, ACS Nano 4 (2010) 4324–4330.
[41] R. Haul, S.J. Gregg, K.S.W. Sing, Berichte der Bunsengesellschaft für physikalische Chemie 86 (1982) 957.
[42] S. Indrawirawan, H. Sun, X. Duan, S. Wang, J. Mater. Chem. 3 (2015) 3432–3440.
[43] J. Iqbal, T. Jan, S. Ul-Hassan, I. Ahmed, Q. Mansoor, M. Umair Ali, F. Abbas, M. Ismail, AIP Adv. 5 (2015) 1–9.
[44] A.C. Ferrari, J. Robertson, Phys. Rev. B 61 (2000) 14095–14107.
[45] P. Iamprasertkun, W. Hirunpinyopas, A. Keerthi, B. Wang, B. Radha, M.A. Bissett, R.A.W. Dryfe, J. Phys. Chem. Lett. 10 (2019) 617–623.
[46] V.C. Tung, M.J. Allen, Y. Yang, R.B. Kaner, Nat. Nanotechnol. 4 (2009) 25–29.

[47] K. Mahmood, S.B. Park, H.J. Sung, J. Mater. Chem. 1 (2013) 3138–3149.
[48] A.P. Litvinchuk, A. Möller, L. Debbichi, P. Krüger, M.N. Iliev, M.M. Gospodinov, J. Phys. Condens. Matter 25 (2013) 105402.
[49] D.P. Volanti, D. Keyson, L.S. Cavalcante, A.Z. Simões, M.R. Joya, E. Longo, J.A. Varela, P.S. Pizani, A.G. Souza, J. Alloys Compd. 459 (2008) 537–542.
[50] P. Gao, F. Li, H. Zhan, N. Zhao, F. Xiao, W. Wei, L. Zhong, H. Wang, Y. Sun, J. Catal. 298 (2013) 51–60.
[51] H. Wilmer, T. Genger, O. Hinrichsen, J. Catal. 215 (2003) 188–198.
[52] S. Natesakhawat, P.R. Ohodnicki Jr, B.H. Howard, J.W. Lekse, J.P. Baltrus, C. Matranga, Top. Catal. 56 (2013) 1752–1763.
[53] Y. Zeng, T. Zhang, Y. Xu, P. Hu, T. Ye, Z. Jia, S. Ju, RSC Adv. 6 (2016) 6737–6746.
[54] T. Witoon, J. Chalorngtham, P. Dumrongbunditkul, M. Chareonpanich, J. Limtrakul, Chem. Eng. J. 293 (2016) 327–336.
[55] W. Fan, Y.-E. Miao, Y. Huang, W.W. Tjiu, T. Liu, RSC Adv. 5 (2015) 9228–9236.
[56] S. Poulston, P.M. Parlett, P. Stone, M. Bowker, Surf. Interface Anal. 24 (1996) 811–820.
[57] O. Lupan, G.A. Emelchenko, V.V. Ursaki, G. Chai, A.N. Redkin, A.N. Gruzintsev, I.M. Tiginyanu, L. Chow, L.K. Ono, B. Roldan Cuenya, H. Heinrich, E.E. Yakimov, Mater. Res. Bull. 45 (2010) 1026–1032.
[58] D. Guo, R. Shibuya, C. Akiba, S. Saji, T. Kondo, J. Nakamura, Science 351 (2016) 361.
[59] Y. Qin, J. Yuan, J. Li, D. Chen, Y. Kong, F. Chu, Y. Tao, M. Liu, Adv. Mater. 27 (2015) 5171–5175.
[60] R.I. Jafri, N. Rajalakshmi, K.S. Dhathathreyan, S. Ramaprabhu, Int. J. Hydrogen Energy 40 (2015) 4337–4348.
[61] S. Maldonado, S. Morin, K.J. Stevenson, Carbon 44 (2006) 1429–1437.
[62] J.D. Wiggins-Camacho, K.J. Stevenson, J. Phys. Chem. C 113 (2009) 19082–19090.
[63] R. Liu, F. Li, C. Chen, Q. Song, N. Zhao, F. Xiao, Catal. Sci. Technol. 7 (2017) 1217–1226.
[64] Y. Zhang, C. Chen, X. Lin, D. Li, X. Chen, Y. Zhan, Q. Zheng, Int. J. Hydrogen Energy 39 (2014) 3746–3754.
[65] I. Ud Din, M.S. Shaharun, D. Subbarao, A. Naeem, J. Power Sources 274 (2015) 619–628.
[66] A. García-Trenco, A. Martínez, Catal. Today 215 (2013) 152–161.
[67] X. Li, H. Wang, J.T. Robinson, H. Sanchez, G. Diankov, H. Dai, J. Am. Chem. Soc. 131 (2009) 15939–15944.
[68] H. Ren, C.-H. Xu, H.-Y. Zhao, Y.-X. Wang, J. Liu, J.-Y. Liu, J. Ind. Eng. Chem. 28 (2015) 261–267.
[69] K. Sun, Z. Fan, J. Ye, J. Yan, Q. Ge, Y. Li, W. He, W. Yang, C.-j. Liu, J. CO_2 Util. 12 (2015) 1–6.
[70] J. Xiao, D. Mao, X. Guo, J. Yu, Energy Technol. 3 (2014) 32–39.
[71] J. Toyir, P. Ramírez de la Piscina, J.L.G. Fierro, Ns. Homs, Appl. Catal. B 34 (2001) 255–266.
[72] X.-M. Liu, G.Q. Lu, Z.-F. Yan, Appl. Catal. A 279 (2005) 241–245.
[73] X. Guo, D. Mao, G. Lu, S. Wang, G. Wu, J. Catal. 271 (2010) 178–185.
[74] G. Wang, L. Chen, Y. Sun, J. Wu, M. Fu, D. Ye, RSC Adv. 5 (2015) 45320–45330.